Modeling DSC Melting Curves of Isotactic Polypropylene – Source of Information on Isospecificity of Active Centers

Yury V. Kissin*

Rutgers, The State University of New Jersey, Department of Chemistry and Chemical Biology, 610 Taylor Road, Piscataway, New Jersey, 08854, USA

Abstract: A method is developed for modeling DSC melting curves of isotactic polypropylene produced with single-center and multi-center Ziegler-Natta catalysts. The modeling demonstrates that the use of a simple statistical model of an imperfectly isotactic polymer and the introduction of several assumptions about the crystallization pattern of isotactic blocks in propylene polymers are sufficient for the representation of most characteristic features of their DSC melting curves. This type of modeling can be a source of information on the distribution of active centers with respect to isospecificity. Several examples demonstrate the utility of this modeling approach.

Keywords: Differential canning calorimetry (DSC), melting point, crystallization, polypropylene (PP), Ziegler-Natta catalysts.

INTRODUCTION

Differential scanning calorimetry (DSC) is widely used for characterization of semi-crystalline olefin polymers such as polyethylene and ethylene/α-olefin copolymers [1-3], isotactic and syndiotactic polypropylene (PP) [1-e,2,4-a,5-8], propylene/α-olefin copolymers [4-b,9], and polymers of higher α-olefins and styrene [2,10]

Numerous earlier studies have shown that interpretation of DSC curves of isotactic PP is a complex subject. As soon as modern high-resolution DSC instruments became available, it became obvious that melting curves of isotactic PP produced with heterogeneous Ziegler-Natta catalysts often contain several closely spaced melting peaks [11-17]. Multiple melting peaks sometimes appear even on DSC curves of highly crystalline PP samples thoroughly extracted with boiling hydrocarbons to remove small amounts of stereo-irregular material. The peak multiplicity is especially pronounced when the samples are annealed at a single temperature [13-b] or crystallized under step-wise conditions [17-c]. Another factor complicating DSC analysis of isotactic PP is the existence of three crystal forms of the polymer, α, β and γ, each with a characteristic wide-angle x-ray pattern, a different melting point (T_m) and a different melting enthalpy (ΔH_f^o) [12-b,17-c,18-21].

The synthesis of imperfectly isotactic propylene polymers with single-center catalysts (such as isospecific metallocene catalysts) greatly aided in the interpretation of the DSC data. Most such polymers have strongly depressed T_m values compared to those of highly isotactic PP produced with Ti-based Ziegler-Natta catalysts [2,4-a,5,6,22]. A similarly strong depression of T_m was also observed in copolymers of propylene and other α-olefins prepared with isospecific metallocene catalysts [1-e,4-b,9,15-b]. In both these cases, the reason for the T_m depression is obvious, the shortening of isotactic sequences in polymer chains either due to more frequent steric errors (in homopolymers) or due to insertion of α-olefin units in PP chains (in copolymers). On the other hand, T_m values of PP produced with different multi-center Ziegler-Natta catalysts are always relatively high, 160 to 165°C [2,7], but their DSC curves usually contain several closely spaced peaks even when a single PP crystal form is present [12,16].

The usefulness of a relatively simple and inexpensive DSC analysis of PP can be significantly expanded by modeling the melting curves. Thus, the paper discusses modeling the shapes of DSC melting curves of imperfectly isotactic PP produced with single-center and various multi-center polymerization catalysts. The principal goal of the article is to demonstrate that the presence of multiple melting peaks on DSC melting curves of PP produced with different multi-center Ziegler-Natta catalysts is caused by steric inhomogeneity of the polymers, i.e., by the presence in them of several components with a different (although usually all very high) degree of isotacticity. Within this interpretation, positions of maximums on such DSC melting curves and the widths of melting transitions provide information about the steric purity and steric inhomogeneity of the polymers.

*Address correspondence to this author at the Rutgers, The State University of New Jersey, Department of Chemistry and Chemical Biology, 610 Taylor Road, Piscataway, New Jersey, 08854, USA; Tel: 1-732-445-5882;
Fax: 1-732-445-5312; E-mail: ykissin@rci.rutgers.edu

E-ISSN: 1929-5995/13

EXPERIMENTAL SECTION

Several PP samples were studied; they all were prepared in the laboratory. The following catalysts were used:

(a) Soluble isospecific metallocene catalyst *rac*-$Me_2Si(4\text{-}Ph\text{-}2\text{-}Me\text{-}Ind)_2ZrCl_2$ - MAO; polymerization at 50°C. Reaction details are given in ref. [23].

(b) Three early heterogeneous catalysts based on γ-$TiCl_3$, δ-$TiCl_3$ and VCl_3 with $Al(C_2H_5)_3$ as a cocatalyst All polymerization reactions were carried out at 70°C at the propylene partial pressure of 3 atm.

(c) Supported polymerization catalyst of the 5th generation [24] containing a diether as an internal donor, $TiCl_4$/2,2-di-*i*-Bu-1,3-$(MeO)_2$-propane/MCl_2, with $Al(C_2H_5)_3$ as a cocatalyst; polymerization at 70°C.

(d) Post-metallocene Ti complex bis-[N-(3,5-di-*t*-Bu-salicylidene)-2,3,5,6-F_4-aniline]$TiCl_2$ activated with a combination of $Al(C_2H_5)_2Cl$ and $Mg(C_4H_9)_2$; polymerization at 50°C [25].

DSC melting curves of the polymers were recorded using DuPont 2200, 9900 DSC Systems, Perkin-Elmer DSC-7 and TA Q200 instruments. In most cases, polymer samples weighing from 5 to 8 mg were first melted by heating to 180°C at a rate of 5 or 10°C min^{-1}, then they were crystallized and annealed by cooling from 180°C to room temperature at a rate of 1°C min^{-1}, and, finally, melting curves of the uniformly crystallized samples were recorded at a rate of 2 or 5°C min^{-1}.

Modeling of melting curves was carried out with the Mathematica 8.0 program.

RESULTS AND DISCUSSION

Modeling DSC Melting Curve of Structurally Uniform Isotactic PP

DSC melting curves of isotactic PP produced with soluble single-center metallocene catalysts are usually relatively narrow and contain a single asymmetric peak (see one example below in Figure **4-A**). T_m values of these polymers depend on the stereoregularity level. For example, a decrease of the fraction of *mmmm* pentads (the most often used ^{13}C NMR parameter of PP isotacticity) from 0.98 to ~0.55 is accompanied by a decrease of T_m from ~163 to ~85°C [2,4-a,5,6,22]. A polymer with the highest experimentally measured [*mmmm*] value of 0.9996 (it was produced with a sterically shielded salalen Ti complex) has the highest experimentally measured T_m, 169.9°C [26]. Its heat of fusion, ΔH_f, is also very high, 104.2 J·g^{-1}.

The reason for this correlation between T_m and [*mmmm*] values is clear: only long isotactic sequences in propylene macromolecules acquire the 3_1 helical conformation and can form crystals. Any interruption in the isotactic linking of propylene units in a polymer chain leads to shortening of isotactic blocks and, as a result, to thinning of the crystalline lamellae. For this reason, modeling of the DSC curve of an imperfectly isotactic polymer starts with the statistical description of a stereoregular polymer chain.

Basic Statistics of Imperfectly Isotactic Polymers

A predominantly isotactic PP macromolecule can be viewed as consisting of sets of isotactic blocks (isotactic monomer sequences) of meso-linked propylene units, (*iso*-P)$_n$. Each such block is flanked by two monomer units in the opposite (racemic) stereo-configuration, as, for example, an (*iso*-P)$_n$ block with n = 10:

┘ ┐ ┐ ┐ ┐ ┐ ┐ ┐ ┐ ┐ ┘ (sequence 1)
r m m m m m m m m m r

Sequence 1 is alternatively represented as rm_9r. The number n of monomer units in an (*iso*-P)$_n$ block can vary starting from two (one meso-link) to any large number.

The mechanism of stereo-control in propylene polymerization reactions with most isospecific catalysts, including bridged metallocene catalysts and common Ziegler-Natta catalysts, can be satisfactorily described by the stereo-site (enantiomorphic) scheme [27]. This mechanism, in its simplest form, is suitable for the description of isospecific active centers with a high to moderate degree of stereo-control. The dominant form of linking of monomer units in a growing polymer chain produced with such active centers is the meso-linking. If, on occasion, a propylene molecule is inserted into a growing polymer chain in the racemic configuration (and, thus, a steric error occurs), the error is corrected immediately, in the next monomer insertion step [28]. Therefore, a segment of an isotactic chain with a single steric error can be represented as:

┐ ┐ ┐ ┐ ┐ ┐ ┘ ┐ ┐ ┐ ┐ ┐ ┐ (sequence 2)
m m m m m m r r´ m m m m m

Sequence 2 (one monomer unit in an inverted position) is the most frequent stereochemical error in such chains; this segment contains two adjacent racemic links, *r* and *r′*.

The formation of such an imperfectly isotactic chain mostly containing isolated stereo-errors can be conveniently described in terms of two conditional probabilities. The probability of the isotactic chain growth (the probability of meso-linking), p_{iso}, is quite high; it would be equal to 1 in the absence of any stereo-errors. The probability of a single stereo-error (the probability of the *r* linking in sequence 2) is $1 - p_{iso}$. The probability of the stereo-corrective step (the probability of the *r′* linking) is high and, in the simplest case, it is assumed to be equal to p_{iso}.

Many physical and mechanical properties of α-olefin polymers, including their crystallinity level, T_m (the subject of this paper), as well as relative absorbances of stereoregularity bands in their IR spectra [28] are determined by the presence of long isotactic sequences that form polymer crystals. Two statistical functions are used to quantify isotactic sequences in imperfectly isotactic chains [1-d,12,28].

1. raction of propylene units in isotactic blocks containing *n* monomer units

$$\delta(iso\text{-P})_n = n \cdot p_{iso}^{\ 2} \cdot (1 - p_{iso})^2 \cdot [p_{iso}^{\ n-2} + (1 - p_{iso})^{n-2}] \approx n \cdot p_{iso}^{\ n} \cdot (1 - p_{iso})^2 \quad (1)$$

2. Fraction of propylene units in the sum of all long isotactic blocks starting with the block containing *n* units, that is, the fraction of propylene units in the sum of blocks $(iso\text{-P})_n$, $(iso\text{-P})_{n+1}$, $(iso\text{-P})_{n+2}$, etc.,

$$\Sigma(iso\text{-P})_n = p_{iso}^{\ n} \cdot [p_{iso}^{\ 2} + (n + 1) \cdot (1 - p_{iso}) + n \cdot (1 - p_{iso})^2] + (1 - p_{iso})^{n} \cdot [p_{iso} \cdot (n + 1) \cdot (1 - p_{iso}) + 1 + n \cdot p_{iso}^{\ 2}] \approx p_{iso}^{\ n} \cdot [p_{iso}^{\ 2} + (n + 1) \cdot (1 - p_{iso}) + n \cdot (1 - p_{iso})^2] \quad (2)$$

Three examples of the $\delta(iso\text{-P})_n$ function are shown in Figure **1**, one for a highly isotactic polymer with p_{iso} = 0.98 and the other two for polymers of moderate isotacticity with p_{iso} = 0.95 and 0.92. It is obvious that most propylene units in all three examples are positioned in long isotactic blocks that account for crystallinity of the polymers. The distribution of propylene units strongly depends on the p_{iso} value: the higher p_{iso}, the higher is the fraction of propylene units in long crystallizable isotactic blocks. In the case of a polymer with p_{iso} = 0.98, the largest fraction of propylene units is in blocks ranging from 50 to 60, for p_{iso} = 0. 95 in blocks from 20 to 25, and for p_{iso} = 0.92 in blocks of ~12 units. It is obvious also that the distribution of the block lengths is quite broad for highly isotactic polymers and is narrower for polymers of a moderate isotacticity level.

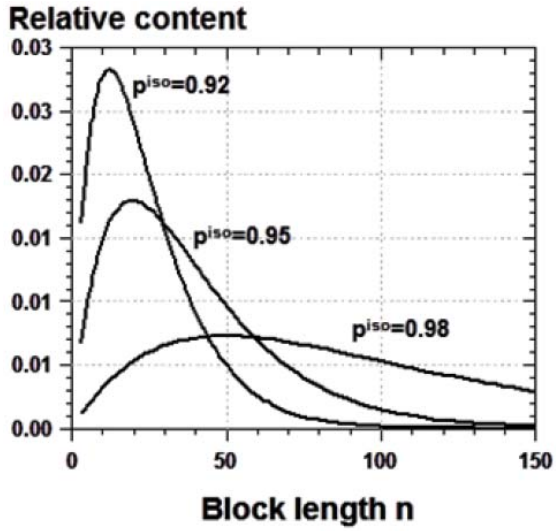

Figure 1: Monomer unit distribution in isotactic blocks of different size in sterically uniform PP of different isotacticity level.

At the present time, the ^{13}C NMR technique is the dominant method for the evaluation of PP stereoregularity. The stereochemical nomenclature of the NMR method has been universally accepted for the description of polymer stereoregularity in general. For example, if a segment of a polymer chain containing a single steric error is described by sequence 2 shown above, the polymer chain contains a single *mrrm* pentad in the center of the segment flanked by two *mmrr* and two *mmmr* pentads. The two most often reported ^{13}C NMR parameters of imperfectly isotactic PP polymers are the contents of iso-triads, [*mm*], and iso-pentads, [*mmmm*]. Their definitions in terms of p_{iso} are [28]:

$$[mm] = p_{iso}^{\ 3} + (1 - p_{iso})^3 \text{ and } [mmmm] = p_{iso}^{\ 5} + (1 - p_{iso})^5 \quad (3)$$

Comparison of Experimental T_m Values and Statistics

Figure **2** shows melting points of a series of structurally uniform PP samples prepared with metallocene catalysts (data from [22]) as a function of p_{iso}. The structural uniformity of such polymers (the same isotacticity level for all the macromolecules in a given polymer) was confirmed by the Tref method [2,29]. The p_{iso} values in Figure **2** were calculated from NMR data using Equation 3.

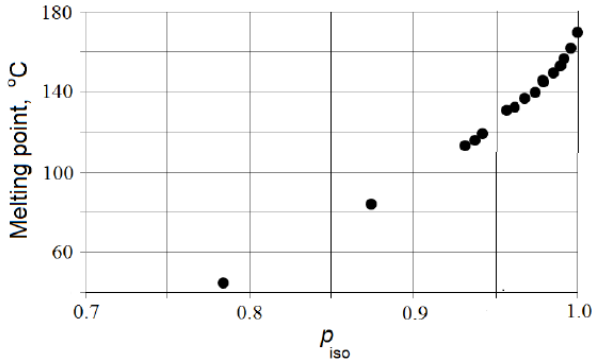

Figure 2: Melting temperatures of PP produced with isospecific metallocene catalysts as a function of p_{iso} value. Experimental data from [22].

As Figure **1** shows, the distribution of propylene units in blocks (*iso*-P)$_n$ of a different size in a sterically uniform polymer has a maximum which corresponds to the size of the "most abundant" isotactic sequence. The position of this maximum as a function of n is determined from Equation 1 at $d[\delta(iso\text{-P})_n]/dn = 0$:

$$n_{max} = -[\ln(p_{iso})]^{-1} \quad (4)$$

As one can expect, n_{max} strongly increases with p_{iso}.

It is very instructive to plot experimentally measured T_m values of isotactic metallocene-catalyzed PP polymers from Figure **2** vs. their n_{max} values calculated from NMR data with Equation 4. This dependence is shown in Figure **3-A**.

The plot has two distinct ranges. The range at the right characterizes polymers with relatively large n_{max} values starting from ~50 and, respectively, polymers with a high isotacticity degree, with [*mmmm*] > 0.90 and p_{iso} > 0.98. Such polymers have high T_m, in the 150 - 165°C range, and their T_m values change only slightly with n_{max}.

Isotactic PP, as well as most semi-crystalline polymers, crystallizes in the lamellar form. The relationship between the lamella thickness l (Å) and the number n of propylene units in it is l (Å) = $l_{step} \cdot n$, where l_{step} = 2.17 Å is the length of one propylene unit in the isotactic chain in the 3_1 helical conformation. In general, the range of high n_{max} values, above ~50 in Figure **3-A**, and the respective l_{max} range, above ~110 Å, is very close to the published median values of the lamella thickness distribution in highly isotactic PP, from 100 to 150 Å [30].

Thus, the range of n_{max} > 50 in Figure **3-A** can be rationalized as the effect of chain folding during crystallization, the same as chain folding in polyethylene and in high molecular weight *n*-alkanes [31]. Figure **1** shows that propylene units are arranged in a variety of isotactic blocks (*iso*-P)$_n$, from very long to quite short, and the distribution of propylene units in the blocks varies depending on the p_{iso} value (Equation 1). The nature and the size of the folds, the loops which connect isotactic sequences in crystalline lamellae, are not uniform. Some loops contain propylene units in the racemic configuration (sequence 2); other loops are the parts of long isotactic blocks themselves. As an additional complication, the thickness of the crystalline lamellae in PP, as well as in other semi-crystalline polyolefins, depends on the rate of crystallization from the melt.

The left side of Figure **3-A** characterizes melting of PP polymers with n_{max} < 50, and, respectively, with p_{iso} below 0.98. Melting points of these polymers sharply decrease as the n_{max} value decreases. These n_{max} values are all lower than the average number of monomer units in the lamellae of highly isotactic PP and one can assume that such shorter isotactic

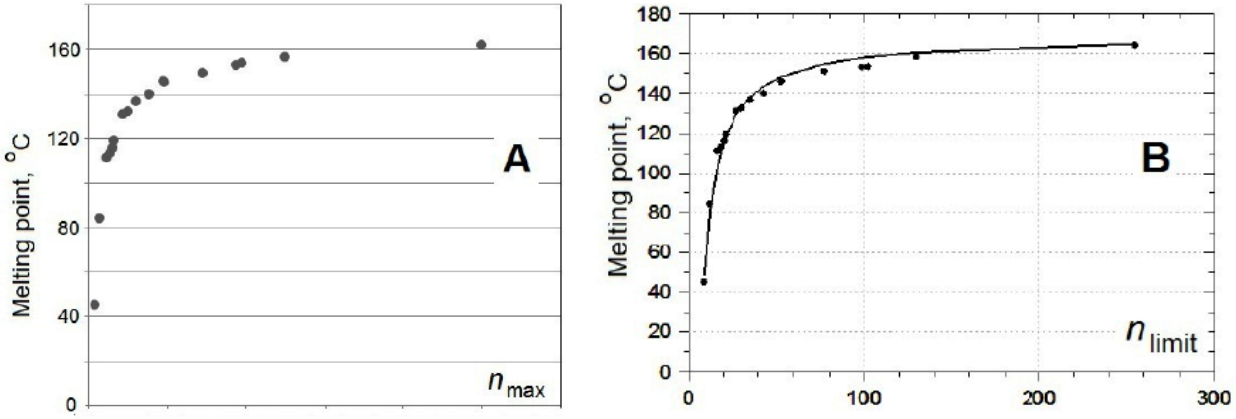

Figure 3: A - Melting temperatures (from Figure **2**) vs. the size of the most abundant propylene block in PP (calculated with Equation 4). **B** - Experimental data from Figure **3-A** in coordinates of Equation 6.

Table 1: Crystallization of Different Isotactic Blocks in Sterically Uniform PP

Isotactic blocks (*iso*-P)$_n$	Content	Type of crystallization
Long crystallizable blocks, $n \geq n_{limit}$	Equation 2	Primary, at high temperatures. *Model 1*, Equation 11.
Short crystallizable blocks, $n_{limit} > n > n_{min}$	Equation 1	Secondary, at low temperatures. *Model 2* , Equation 12.
Short non-crystallizable blocks, $n \leq n_{min}$	Equation 2, n_{min} = 8 - 9	Blocks are too short to crystallize at 20°C

sequences mostly crystallize in the fully extended form, similarly to crystallization of short *n*-paraffins [31].

Two-Stage Crystallization Process

When a sterically uniform, imperfectly isotactic polymer is slowly crystallized from the melt at a gradually decreasing temperature and then slowly annealed (when the crystallized sample continues to cool), the following sequence of events takes place (Table **1**). Early in the crystallization process, at relatively high temperatures, all long isotactic blocks with *n* higher than a particular n_{limit} value (the value we assume to be very close to n_{max} value) rapidly crystallize in the chain-folded morphology and provide the framework for the spherulite structure.

After crystallization of long propylene blocks into lamellae with folded chains is completed and while the temperature of the polymer sample continues to decrease, secondary crystallization of the remaining shorter (*iso*-P)$_n$ blocks begins. These propylene blocks mostly crystallize in the fully extended form and produce thin lamellae. Finally, very short propylene blocks with *n* lower than a particular minimum *n* value, n_{min}, do not crystallize when the samples are cooled to room temperature, although some of them can be forced to crystallize at lower temperatures.

Below, the two stages of the crystallization and subsequent melting behavior are discussed separately. Model 1 provides a quantitative melting model of chain-folded lamellae containing long isotactic blocks, the range of high n_{max} values in Figure **3-A**. Model 2 gives the melting model of thin lamellae formed in the process of secondary crystallization when the dominant factor determining the T_m value is the total length of crystallizable (*iso*-P)$_n$ blocks, the range of low n_{max} values.

Dependence Between Melting Temperature and Lamella Thickness

In general, the dependence between the equilibrium melting temperature of a polymer lamella, T_m, and the crystal thickness (lamella thickness *l* corresponding to the number of monomer units $n = l/l_{step}$) is usually described by the Thompson-Gibbs equation [31-d]:

$$T_m\,(K) = T_m^o \cdot (1 - \chi/l) = T_m^o \cdot [1 - (\chi/l_{step})/n)] \quad (5)$$

The T_m^o value in Equation 5 is the equilibrium melting temperature of the infinitely thick lamellar crystal. Various estimations for isotactic PP give greatly varying T_m^o values, from 443 to 493K [2,4-a,11,13-b,19,22,26,32]. The χ parameter in Equation 5 is a constant related to the free energy of the fold surface and the bulk free energy of fusion [10-b,31-b,31-d].

The practice of DSC analysis is far removed from equilibrium conditions of crystallization and melting. All the DSC steps are carried out non-isothermally. Therefore, several empirical parameters should be introduced when crystallization and melting of PP with different p_{iso} values is modeled. In particular, the T_m value of a given polymer depends on the heating rate: the higher the rate the higher is T_m. In practice, the T_m^o value is determined empirically, as a limit T_m value for a perfectly isotactic polymer (a polymer with $p_{iso} \approx 1.0$) measured under given DSC recording conditions. The χ value also depends on the crystallization conditions and cannot be independently estimated either. Instead, empirical expressions are usually used to describe experimental T_m vs. *l* data.

Equation 5 holds when all the lamellae have the same thickness *l*. Of course, real PP polymers have isotactic blocks of a widely varying length (Figure **1**) and the n_{max} value characterizes the <u>average</u> lamella thickness, $l_{av} = l_{step} \cdot n_{max}$. Several computational trials showed that the utility of Equation 5 for the description of experimental data in Figure **3-A** can be improved if one assumes that the average thickness of the lamellae formed in the process of the primary crystallization is slightly higher than $l_{step} \cdot n_{max}$ and can be represented as $l_{av} = l_{step} \cdot n_{limit} = l_{step} \cdot (n_{max} + \varphi)$ where $\varphi \approx 2.5$. The introduced correction is quite small in the case of highly isotactic polymers: the n_{limit}/n_{max} ratio is

merely ~1.02 at p_{iso} = 0.99, ~1.04 at p_{iso} = 0.98 and ~1.1 at p_{iso} = 0.96.

Thus, Equation 5 for isotactic PP can be rewritten as:

$$T_m\,(K) \approx T_m^o \cdot [1 - (\chi/l_{step})/n_{limit})] \approx T_m^o \cdot \{1 - (\chi/l_{step})/(n_{max} + \varphi)]\} \quad (6)$$

Equation 6 should be regarded as semi-empirical. Its main advantage is its suitability for presenting the T_m vs. n_{max} dependence (such as the one in Figure **3-A**) in a unified way in the whole range of n_{max} values. The only objective applicability criterion of Equation 6 is the estimation of T_m^o; it should be close to the highest experimentally measured T_m, ~443K [26].

Parameters in Equation 6. Figure **3-B** shows the best fit for the experimental data from Figure **3-A** in the coordinates of Equation 6, T_m vs. n_{limit} (solid line); it was calculated using the program Scientist (MicroMath). The parameters of the calculated curve are: T_m^o = 442K, χ= 5.33, l_{step} = 2.17. Unfortunately, the fit between the experimental data and the calculation is the poorest in the n_{limit} range between ~50 to ~120, the range typical for many highly isotactic polymers. However, the fit in this n_{limit} range can be significantly improved by neglecting all the points with n_{limit} <50 (the points for p_{iso} <0.985). This, much better fit is only suited for highly isotactic PP materials with T_m >150°C; it gives the following parameters in Equation 6: T_m^o = 442K (the same as in Figure **3-B**), χ = 6.105. The second part of the experimental curve in Figure **3-A**, the points for T_m <150°C, is also well represented by Equation 6 but with different parameters, T_m^o = 434K, χ = 3.45. Both these latter parameters are strictly empirical; they merely provide a good fit for the data between 40 and 150°C. Some results for the DSC curve resolution presented below give both sets of statistical stereoregularity data (p_{iso} or [*mmmm*] values), one produced with the local calibration for the high n_{limit} range (it gives more precise results for polymers with p_{iso} >0.985) and another, in parentheses, produced with the general calibration curve shown in Figure **3-B**.

Modeling the Shape of DSC Melting Curve of Sterically Uniform, Imperfectly Isotactic PP

Macromolecules of sterically uniform, imperfectly isotactic PP contain both relatively long and relatively short isotactic sequences (Figure **1**). They form two different types of polymer lamellae, relatively thick lamellae formed during the primary crystallization stage and relatively thin lamellae formed during the secondary crystallization age

Models for Two Types of Polymer Lamellae

Model 1 describes melting curves of thick lamellae. The model is based on three assumptions:

1. Long isotactic sequences crystallize in the folded-chain morphology.

2. For a given polymer, there exists an average thickness of the crystalline lamellae, l_{av} (Å), which depends on the isotacticity degree, thermodynamics of chain folding, and on crystallization conditions. The l_{av} value for a sample of imperfectly isotactic PP with a particular thermal history cannot be estimated strictly from the theoretical viewpoint; in can be only evaluated experimentally from the T_m value measured under given DSC conditions (using Equation 6). When such lamellae are subsequently melted, their T_m^{av} value is lower than T_m^o for perfectly isotactic PP with p_{iso} = 1.0 because the l_{av} value for the lamella is smaller than that for perfectly isotactic PP.

3. The thickness of different chain-folded lamellae is not strictly uniform. Model 1 assumes that *l* is distributed according to the Gauss equation with a center at l_{av}:

$$Fr(l) = [\sigma \cdot (2\pi)^{0.5}]^{-1} \cdot Exp[-(l_{av} - l)^2/2\sigma^2] \quad (7)$$

or, in terms of the number of monomer units, $n_{av} = l_{av}/l_{step}$,

$$Fr(n) = [\sigma \cdot (2\pi)^{0.5}]^{-1} \cdot Exp[-l_{step}^2 \cdot (n_{limit} - n)^2/2\sigma^2] \quad (8)$$

where Fr(*n*) is the fraction of lamellae containing *n* monomer units and σ is the width of the lamella thickness distribution. This assumption is based on the fact that DSC melting curves of nearly perfectly isotactic PP have a significant width, 7 - 8°C [26], which is higher than the widths of DSC melting curves of low molecular weight organic crystals.

Plotting Fr(*n*) vs. *n* using Equation 8 gives a symmetrical Gauss curve with the maximum at n_{limit}. However, DSC melting curves are plotted in the coordinates "heat flow ($W \cdot g^{-1}$) or heat capacity ($J \cdot K^{-1} \cdot mol^{-1}$) vs. temperature *T*". This peculiarity of the DSC coordinates calls for a re-formulation of the Gauss function; the required function is "Fr(*n*) vs. temperature *T*" instead of "Fr(*n*) vs. *n*" as given by Equation 8. This

change is implemented using the following general expression [3]:

$$Fr(n) = \Delta H \cdot [dT/dn] \quad (9)$$

where ΔH is the relative apparent heat of fusion at a given T.

The dT/dn term in Equation 8 is produced by differentiating Equation 5:

$$dT/dn = T_m^o \cdot (\chi/l_{step})/n^2 \quad (10)$$

Introducing Equations 9 and 10 into Equation 8 and replacing n with $T_m^o \cdot (\chi/l_{step})/(T_m^o - T)$ from Equation 5 gives the final expression for the shape of the melting curve of chain-folded lamellae of isotactic PP in the DSC coordinates:

$$\Delta H_{Model\ 1} = T_m^o \cdot (\chi/l_{step})/[(T_m^o - T)^2 \cdot (\sigma\sqrt{2\pi})] \cdot$$

$$Exp\{-[T_m^o \cdot (\chi/l_{step})/2\sigma]^2 \cdot [(T_m^o - T_m^{av})^{-1} - (T_m^o - T)^{-1}]^2\} \text{ vs. } T \text{ (K)} \quad (11)$$

The dimension of $\Delta H_{Model\ 1}$ in Equation 11 is K^{-1}; it is normalized to 1, i.e., $\int \Delta H_{Model\ 1} \cdot dT$ over the whole T range is ~1 (all the heat required to melt the weight unit of thick polypropylene crystals).

Model 2 describes melting of crystals which are formed by short isotactic blocks during the secondary crystallization stage. The size range of the short blocks is $n_{limit} > n > n_{min}$. The fraction of propylene units in each short block is given by Equation 1. The model is based on the following assumptions:

1. Comparing n values in this range, which vary from ~50 to ~10 - 20, with an average equilibrium lamella size for highly isotactic PP [30], n = 50 - 60, one can assume that these short propylene sequences crystallize in the fully extended form. Surfaces of these thin lamellae do not contain tightly folded isotactic segments; they consist of monomer units in the racemic configuration and adjacent meso-linked units (sequence 2) as well as end-groups of polymer chains.

2. As the first approximation, each short propylene block with $n_{limit} > n > n_{min}$, if it is crystallized at a slowly decreasing temperature, co-crystallizes only with propylene blocks of approximately the same size and they form lamellae of a relatively uniform thickness. Within this approximation, the fraction of propylene units in the $(iso\text{-P})_n$ block, the $\delta(iso\text{-P})_n$ value in Equation 1, determines the fraction of these units in lamellae with the thickness $l_{step} \cdot n$ (Å).

If one assumes that the heat of fusion per one propylene unit does not depend on lamella thickness, the second assumption in Model 2 signifies that the heat flow is proportional to the $\delta(iso\text{-P})_n$ value (Figure **1**). As stated above, DSC melting curves are plotted in the coordinates "heat flow vs. temperature". Thus, to produce a theoretical DSC melting curve for short lamellae, one has to change the abscissa in Figure **1**; it should be "$\delta(iso\text{-P})_n$ vs. T" instead of "$\delta(iso\text{-P})_n$ vs. n", the same transformation as in Model 1. This substitution is also achieved by using Equations 9 and 10, as above. Following the same procedure as that used for the derivation of Equation 11, the final expression for the shape of the DSC melting curve of thin secondary crystals in Model 2 is produced:

$$\Delta H_{Model\ 2} = (1 - p_{iso})^2 \cdot (T_m^o \cdot \chi)^2 \cdot (T_m^o - T)^{-3} \cdot p_{iso}^{\theta} \text{ vs. } T \text{ (K)} \quad (12)$$

where $\theta = T_m^o \cdot \chi/(T_m^o - T)$. Formally, the $\Delta H_{Model\ 2}$ value increases with temperature, as Equation 12 predicts, and ends at a temperature corresponding to n_{limit}. To avoid the step-wise change in the shape of the curve, the $\Delta H_{Model\ 2}$ curve is artificially extended to higher temperatures beyond the point of n_{limit}, either as an exponential function $Exp(-k \cdot T)$ or as a hyperbolic tangent function of T with adjustable parameters.

To produce a combined model of the DSC melting curve of a sterically uniform PP, Equations 11 and 12 should be combined proportionally to the fractions of propylene units in the respective long and short sequences:

$$\Delta H_{combined} \approx \Sigma(iso\text{-P})_n \cdot \Delta H_{Model\ 1} + \Delta H_{Model\ 2} \text{ vs. } T \text{ (K)} \quad (13)$$

where n in the first term is n_{limit} and the contribution of the second term is calculated only from n_{min} to n_{limit}. The dimension of $\Delta H_{combined}$ is also K^{-1}; it is normalized to 1, i.e., $\int \Delta H_{combined} \cdot dT$ over the whole temperature range is ~1; i.e., it is the combined heat spent to melt the weight unit of a mixture of both types of polypropylene crystals, primary (thick) and secondary (thin).

To convert the $\Delta H_{combined}$ value to the standard parameter of the DSC ordinate, the specific heat flow (dimension $W \cdot g^{-1} = J \cdot s^{-1} \cdot g^{-1}$) one has to know the sample weight, the heating rate R at the melting stage

($K \cdot s^{-1}$), and the area under the melting curve per g of PP (the heat of fusion, ΔH_f, $J \cdot g^{-1}$). The latter value is routinely calculated as one of the results of a DSC measurement. Thus, the ordinate of the modeled DSC curve should be:

$$\text{Heat flow } (W \cdot g^{-1}) = \Delta H_f \cdot R \cdot \Delta H_{combined} \quad (14)$$

To avoid uncertainties related to heating rates in different DSC experiments and differences in the crystallinity degree of different PP samples (which are proportional to the ΔH_f value), the modeling of DSC melting curves described below was carried out with Equation 13 instead of Equation 14. The ordinate in all the modeled curves shown below is $\Delta H_{combined}$ (K^{-1}).

Polypropylene Produced with Single-Center Isospecific Metallocene Catalyst

Sterically uniform PP materials of high but imperfect isotacticity ($0.98 < p_{iso} < 1$) are produced with some single-center polymerization catalysts based on metallocene and post-metallocene complexes. Figure **4** compares two DSC melting curves of isotactic PP. Figure **4-A** shows the experimental melting curve of a polymer prepared with a highly isospecific metallocene catalyst at 50°C [33]. Judging by the M_w/M_n ratio of the polymer, ~2.5, it is produced with practically a single-center catalyst. High isospecificity of the sample explains both its relatively high T_m, ~161°C, and a high crystallinity degree, 65% [33]. Such narrow melting curves of sterically uniform PP materials are typical for other polymers produced with isospecific single-center metallocene catalysts as well [34] provided that polymer samples were pre-melted and crystallized before DSC recording.

The curve in Figure **4-B** was calculated with Equation 13 using a single parameter p_{iso} = 0.992, it corresponds to [*mmmm*] = 0.961. The average number of propylene units in long crystallizable blocks in this polymer is ~130 and the calculated position of the DSC peak maximum is ~161°C. The effective σ value in Equation 11, ~30, is a combination of two numbers, the instrumental broadening (which is specific for a particular DSC instrument and for particular experimental conditions) and the real σ value in Equation 5 characterizing the distribution of the lamella thickness. Two components in Figure **4-B** show melting curves of long lamellae consisting of folded isotactic chains (curve 1) and shorter lamellae formed in the process of secondary crystallization (curve 2).

A comparison of Figures **4-A** and **4-B** shows that Equation 13 correctly describes the specific asymmetric shape of the melting curve of sterically uniform, imperfectly isotactic PP.

Several points should be made with respect to the use of Models 1 and 2 for PP:

1. Due to the nature of Equation 11, plotting a Gauss curve in the DSC coordinates results in a shift of the curve's maximum: T_m values calculated with Equation 11 are 0.7 - 2.5°C higher than the T_m values used in the calculations; the shift is ~2°C in Figure **4-B**. The exact position of the DSC peak maximum can be calculated from the n_{limit} value. The equation for this calculation is given in Appendix. This peculiarity of Equation 10 signifies that real T_m^{av} values of PP with high [*mmmm*] values are

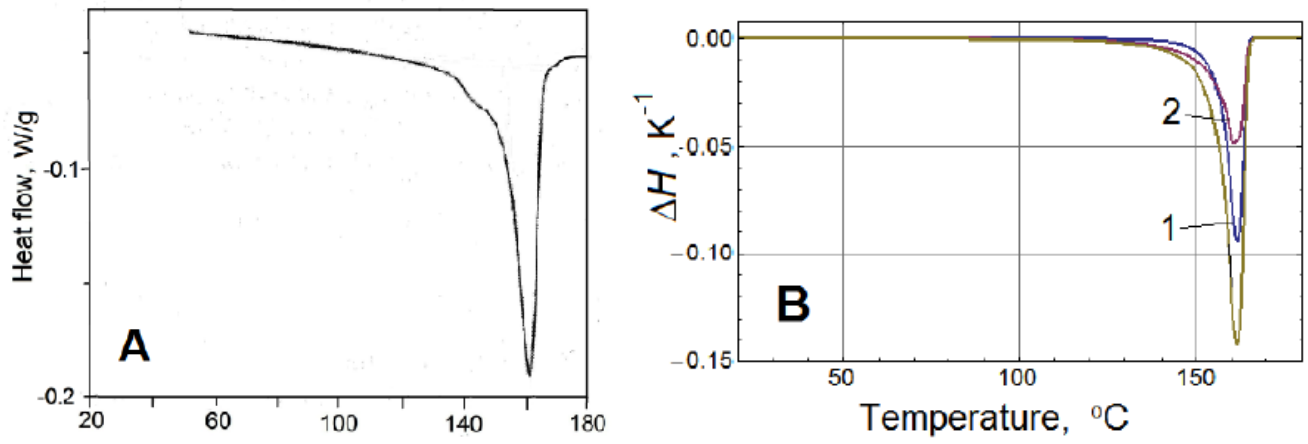

Figure 4: Modeling melting curve of sterically uniform isotactic PP using Models 1 and 2. **A** - Experimental melting curve of PP produced with isospecific single-center metallocene catalyst. **B** - Modeling with Equation 11 (curve 1), Equation 12 (curve 2) and Equation 13 (see text for details).

slightly lower than the temperatures at the maximums of their DSC curves.

2. Due to the nature of Equation 11, the effective width of the calculated peak significantly decreases as T_m^{av} approaches the T_m^o value. To compensate for this change, an artificial increase of the σ value can be introduced into Equation 11 to produce modeled DSC curves with realistic widths.

3. The distortion of the Gauss distribution in the DSC coordinates described by Equation 11 and obvious from Figure **4-B** results in a noticeable difference in the shape of the two sides of the calculated melting curve. The shape of the curve at temperatures below the maximum is determined by the existence of thinner than average lamellae with folded chains (Model 1) and by melting of thin lamellae formed during the secondary crystallization stage (Model 2). On the other hand, the presence of thicker than average lamellae with folded chains, which melt at temperatures above the curve's maximum, is virtually unnoticed in the DSC coordinates.

4. In the literature, the onset of the melting curve, which is defined as an intercept of the tangent to the low-temperature side of the melting curve and its baseline, is often used as the position of "T_m". However, the third assumption of Model 1, the existence of a distribution in the lamella thickness, and the secondary crystallization process described by Model 2 do not justify this practice because the shape of the low-temperature side of a DSC melting curve is mostly determined by melting of thinner lamellae. Positioning the tangent to a DSC melting curve is arbitrary.

Inspection of Figure **4** shows one clear difference between the experimental and the calculated curves: the experimental curve in Figure **4-A** has a shoulder at ~140°C. A possible reason for this shoulder can be less-than-perfect steric uniformity of the polymer. Some minor active centers are usually present in such catalyst systems, most probably the centers derived from *meso*-isomers of the metallocene complexes [33]. Such centers can produce small amounts of PP with a much lower isotacticity degree. These shoulders on DSC curves of metallocene-catalyzed PP polymers were reported earlier [19] but only at very high cooling rates when the γ-crystalline type of PP can form.

DSC melting curves of PP samples of low isotacticity, with $p_{iso} < 0.98$ and with $T_m < 140$°C, can be described exclusively by Model 2. Such polymers are prepared with a variety of metallocene and post-metallocene catalysts of low isospecificity. According to Model 2, crystallites of such polymers do not contain any folded isotactic segments. Lamellae in such polymers are formed by all relatively short isotactic segments (*iso*-P)$_n$ in the extended conformation. The distribution of the lamella thickness for such thin lamellae is given by Equation 1 and its transformation in the GPC coordinates by Equation 12 for all n starting with n_{min}.

Modeling DSC Melting Curves of Multi-Component PP

Polypropylene Produced with Multi-Center Post-Metallocene Catalyst

The use of post-metallocene catalysts of low isospecificity provides several clear examples of PP mixtures containing fractions with different isotacticity levels. Figure **5-A** shows the DSC melting curve of a PP sample prepared with a post-metallocene catalyst [25]. This polymer can serve as a structural opposite to

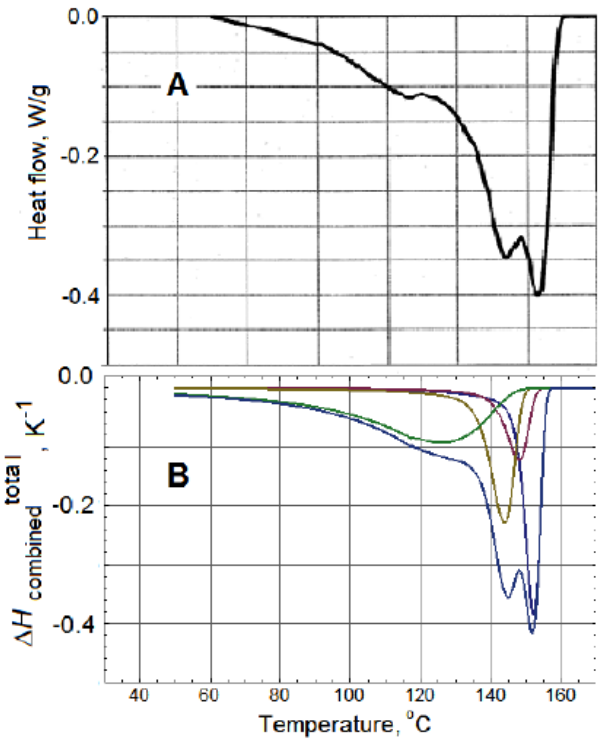

Figure 5: Modeling melting curve of sterically nonuniform isotactic PP. **A** - Experimental melting curve of PP prepared with post-metallocene catalyst [25]. **B** - Modeling with four components, three described by Equation 13 and one (broad) by Equation 12.

that shown in Figure **4-A**, i.e., a propylene polymer with a very complex melting behavior. The polymer contains ~35% of the heptane-insoluble crystalline fraction. The average [*mmmm*] value of the unfractionated product is merely ~0.35, its crystallinity degree and the ΔH_f value are also low, ~10% and ~17 $J \cdot g^{-1}$, respectively. Three crystalline components are observable; their T_m values are, respectively, 153, 144 and ~125°C.

Figure **5-B** shows the results of DSC modeling for this polymer mixture. It was mostly carried out by a trial-and-error method. To achieve a good fit, one has to assume that four components of a different isotaciticity degree are present in the mixture. The $\Delta H_{combined,i}$ value for each of the four components *i* was calculated with Equation 13 and the combined modeled DSC curve was calculated as:

$$\Delta H_{combined}^{total} = \Sigma(Fr_i \cdot \Delta H_{combined,i}) \text{ vs. } T \text{ (K)} \quad (15)$$

where Fr_i is the weight fraction of the *i* component. Table **2** lists parameters of the four components and the Fr_i values. It seems reasonable to assume that these DSC peaks represent separate PP components in the polymer mixture, which are formed by active centers of a different isospecificity level.

Polypropylene Produced with Multi-Center Supported Ziegler-Natta Catalyst

It was noticed long ago that propylene polymers prepared with Ti-based Ziegler-Natta catalysts, which account for the overwhelming majority of all commodity PP resins, have relatively broad DSC melting curves which sometimes consist of two or three distinct components [11-17]. The presence of several components is especially noticeable when the melting curves of slowly crystallized/annealed samples are recorded at low heating rates. The original explanation of the multi-peak phenomenon was based on a premise that these polymer materials, after fractions of decreased stereoregularity were removed from them by extraction with boiling solvents (*n*-heptane or toluene) were nearly perfectly isotactic. Therefore, the appearance of several melting peaks was interpreted as a manifestation of some purely physical phenomena, such as complex crystallization/ recrystallization processes of the α-form of isotactic PP, a function of crystallization and annealing temperatures [12-b]. However, such clear effects of crystallization conditions on the development of multiple peaks were found experimentally only when single- or multiple-point isothermal annealing steps were introduced [13-b,17-c].

More recent ^{13}C NMR, Crystaf and Tref data have revealed that isotacticity level of PP polymers produced with Ziegler-Natta catalysts, although very high, is not perfect and that their chains contain the same stereo-errors (sequence 2) as those found in PP produced with metallocene catalysts [2]. These errors are present in different (but always small) amounts in different components in the polymers. Tref analysis provided the most detailed information on the subject. It showed that these polymers are in reality multi-component mixtures containing, in comparable amounts, fractions of different stereoregularity and molecular weight [2,28,29,35]. Each such polymer component is produced by a particular population of active centers in the catalyst. The number of the components usually ranges from four to six.

Table **3** gives one example, the Tref data for PP prepared with a supported Ti-based Ziegler-Natta catalyst of the 5th generation [35]. The data demonstrate measurable differences between p_{iso} and [*mmmm*] values of Tref-separated components in this polymer. All the components are highly isotactic, especially the two dominant ones, components 1 and 2, which are present in the polymer in comparable amounts.

In the current study, this conclusion was further supported by Crystaf data for a similarly prepared PP with M_w = 129,500, M_w/M_n = 3.7, $[mmmm]_{av}$ = 0.972.

Table 2: Parameters of DSC Components in PP Prepared with Post-Metallocene Catalyst (Figure 5-B)

Component	*I*	*II*	*III*	*IV*
p_{iso}	0.984	0.979	0.975	0.945
[*mmmm*]	0.920	0.899	0.881	0.754
Fr, %	25	11	22	42
σ	9.0	7.5	5.5	10.0
T_m (DSC)	152	148	144	130
n_{limit}	63	50	42	21

Table 3: Parameters of Analytical Tref Components in PP[a)] Prepared with Ziegler-Natta Catalyst of 5th Generation

Tref component	T_{cryst}, °C	p_{iso}	[*mmmm*]	*Fr*, %
1	113.2	0.996	0.979	32.7
2	112.0	0.995	0.975	47.5
3	108.6	0.992	0.963	5.9
4	104.8	0.990	0.950	11.3
5	100.8	0.987	0.935	2.6

[a]Average parameters: M_w = 258,800, M_w/M_n = 6.4, I.I. = 91.7%, [*mmmm*] = 0.972 (^{13}C NMR data).

Figure **6** shows the Crystaf curve of this polymer and its resolution into individual components. The procedure for the resolution was similar to that described earlier for the Crystaf analysis of ethylene/α-olefin copolymers [36].

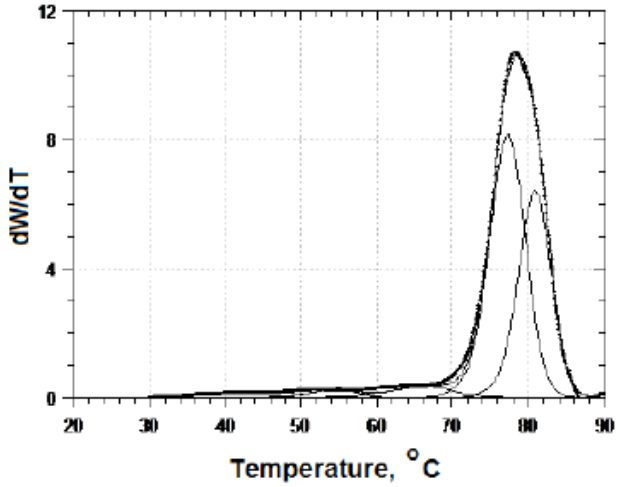

Figure 6: Tref curve of PP prepared with isospecific supported Ziegler-Natta catalyst at 70°C and its resolution into individual components.

According to the Crystaf data, this polymer contains four components, which crystallize from solution in 1,2,4-trichlorobenzene at 81.0, 77.4, 66.4 and ~55°C, respectively. Two dominant components, which crystallize at the highest temperatures, account for ~39 and 55% of the total polymer, whereas the two other components, which crystallize at lower temperatures, are minor, ~3.5 and 2%. In the absence of a dependable calibration for the Crystaf analysis of isotactic PP, the isotacticity level of the Crystaf-separated components can be estimated only approximately from the $[mmmm]_{av}$ value for the total polymer. This estimation gives the [*mmmm*] values for the two dominant Crystaf components as ~0.98 and ~0.97, respectively. Overall, the results of Tref and Crystaf analyses for this PP sample are in a reasonably good agreement.

Figure **7-A** shows the DSC melting curve of the same polymer. It is moderately crystalline; its ΔH_f value is ~66 J·g^{-1}. Because the crystallization/annealing step before the DSC recording was carried out slowly and the DSC heating rate was also low, 2°C min^{-1}, the melting curve exhibits a clear structure whereas a DSC recording at a higher heating rate would produce a single medium-broad melting peak. The melting curve in Figure **7-A** was resolved into several components, each with the shape given by Equation 13. The results of the resolution are shown in Figure **7-B**. At this stage, the resolution is strictly formal: any DSC curve with several partially overlapping components can be, in principle, resolved into elementary components using Equations 13 and 14.

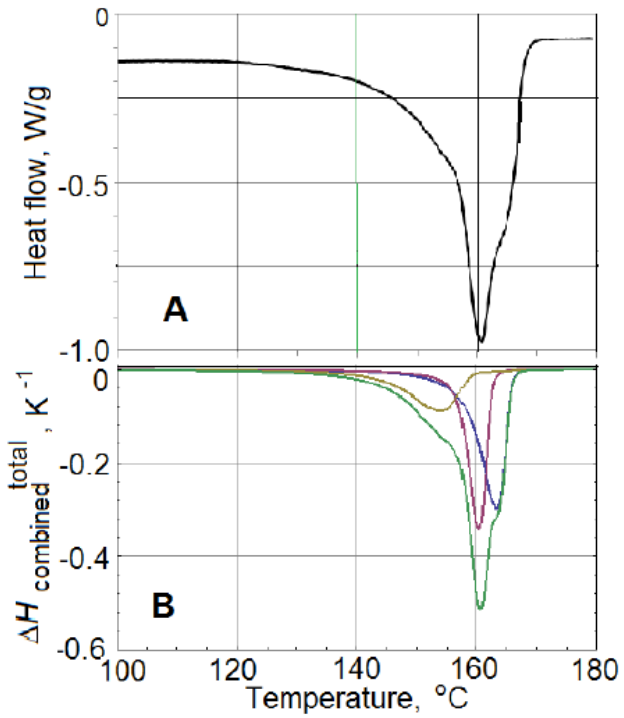

Figure 7: Modeling melting curve of sterically nonuniform isotactic PP. **A** - Experimental melting curve of PP prepared with isospecific supported Ziegler-Natta catalyst. **B** - Modeling with Equation 15; three isotactic components, each described by Equation 13.

Table 4: Modeling DSC Curves of PP Prepared with Supported Ziegler-Natta Catalyst of 5th Generation (Figure 7-B)

Component	T_m, °C	p_{iso}	[*mmmm*]	n_{max}	*Fr*, %
I	163.4	0.994 (0.993)	0.971 (0.967)	175 (320)	38.2 (40.6)
II	160.4	0.992 (0.992)	0.962 (0.958)	134 (223)	38.2 (34.4)
III	154.1	~0.983	0.916	65	13.5

Table **4** lists parameters of DSC components from Figure **7-B**. Their comparison with the Tref data in Table **3** and with the Crystaf data in Figure **6** strengthens the assertion that individual peaks on DSC curves of PP prepared with multi-center catalysts can be ascribed to crystallization and melting of individual polymer components of different isotacticity In other words, DSC analysis of PP samples, if performed at relatively low cooling and heating rates, represents an additional tool for probing structural uniformity of PP materials, similarly to Tref and Crystaf methods.

The following conclusions can be made about the nature of the polymer produced with the supported multi-component Ziegler-Natta catalyst:

1. Overall, the statistical results, p_{iso} and [*mmmm*] values, are similar for different types of analysis, although they were determined completely independently, from ^{13}C NMR of unfractionated samples in Tref analysis [35] (Table **3**) and from the T_m vs. n_{limit} dependence in DSC analysis described by Equation 5.

2. The polymer contains two dominant components of a high isotacticity degree, one with p_{iso} ~0.994 and another ~0.992. These components are present in the polymer in comparable amounts (Fr_i). The mixture also contains several smaller component of a lower isotacticity degree, which are not separated by DSC.

3. The isospecificity of the two dominant active centers in the catalyst, although very high, is not as high as that for the dominant centers in some supported catalysts of the 4th generation, where, according to Tref data, the p_{iso} value can reach 0.997 - 0.998, which corresponds to [*mmmm*] = 0.986 - 0.993 [35] .

4. The n_{limit} values for DSC components *I* - *III* in Table **4** are higher than 50 indicating that crystallization of these fractions mostly occurs in the folded-chain morphology.

Polypropylene Produced with Solid Ziegler-Natta Catalysts

Three PP samples were prepared under identical conditions with three classical solid Ziegler-Natta catalysts based on δ-$TiCl_3$, γ-$TiCl_3$ and VCl_3 using $Al(C_2H_5)_3$ as a cocatalyst. DSC curves of the polymers were recorded after removal of atactic components from them with hot *n*-heptane. All three polymers are highly crystalline; their experimentally measured ΔH_f values are, respectively, 89.4, 99.2 and 97.3 $J \cdot g^{-1}$. Resolution of the DSC curves into elementary components is shown in Figures **8** and **9**; parameters of the components are listed in Table **5**.

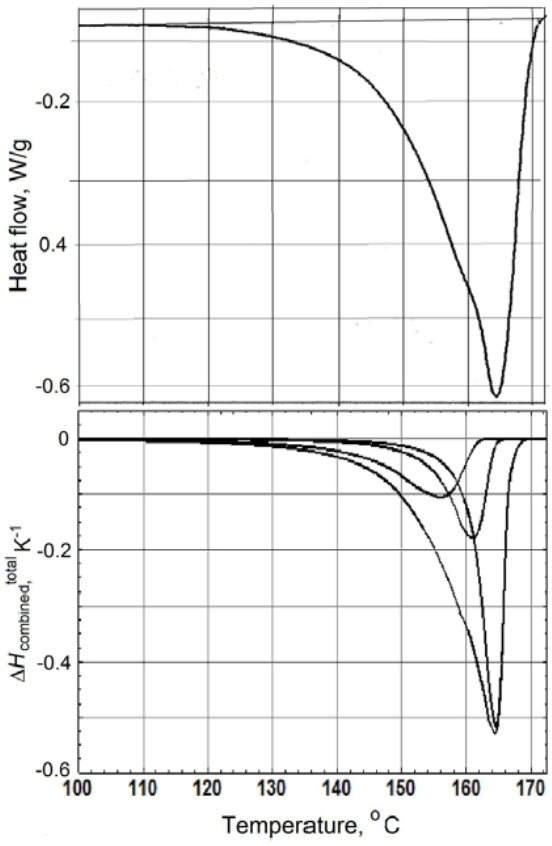

Figure 8: Modeling melting curve of isotactic PP. **A** - Experimental melting curve of PP prepared with Ziegler-Natta catalyst δ-$TiCl_3$ - $Al(C_2H_5)_3$. **B** - Modeling with three components (Equations 13 and 15).

Table 5: Modeling DSC Curves of PP Prepared with Three Solid Ziegler-Natta Catalysts

Catalyst system	Component	T_m, °C	p_{iso}	[*mmmm*]	*Fr*, %
δ-$TiCl_3$ - $Al(C_2H_5)_3$ (Figure **8-B**)	*I*	164.3	0.996 (0.995)	0.978 (0.973)	44.4 (46.5)
	II	160.1	0.992 (0.990)	0.961 (0.951)	26.7 (23.3)
	III	155.6	0.986 (0.980)	0.931 (0.904)	28.9 (30.2)
γ-$TiCl_3$ - $Al(C_2H_5)_3$ (Figure **9-B**)	*I*	162.4	0.994 (0.993)	0.969 (0.965)	22.0
	II	160.4	0.992 (0.990)	0.961 (0.953)	40.7
	III	156.0	0.986 (0.983)	0.931 (0.918)	28.8
	IV	149.2	0.972	0.868	8.5
VCl_3 - $Al(C_2H_5)_3$ (Figure **9-D**)	*I*	161.3	0.992 (0.990)	0.963 (0.952)	28.6
	II	158.3	0.990 (0.989)	0.953 (0.945)	23.8
	III	153.4	0.985 (0.982)	0.927 (0.913)	22.2
	IV	130.6	0.916	0.645	25.4

The component with the highest isotacticity degree among the three analyzed polymers is Component *I* in PP prepared with δ-$TiCl_3$ (Table **5**); p_{iso} = 0.996 and [*mmmm*] = 0.978. In principle, its [*mmmm*] value is only slightly higher than that for Component *I* in PP produced with the supported catalyst (Table **4**, [*mmmm*] = 0.971) and these materials would be very difficult to distinguish by ^{13}C NMR even if they were completely isolated. However, DSC "signatures" of the two components are clearly different; their T_m values differ by nearly 1°C. A similar difference in the isotacticity degree of PP components of the highest isotacticity was noticed earlier in the Tref analysis of polymers prepared with different types of supported catalysts [35]: such a component prepared with the supported catalyst of the 4th generation (utilizing dialkyl phthalate as an internal donor) has a higher isotacticity degree that the same component prepared with a supported catalyst of the 5th generation.

Crystals of δ-$TiCl_3$ and γ-$TiCl_3$ have a different chemical composition (δ-$TiCl_3$ contains from ~33% of Al atoms replacing Ti atoms whereas γ-$TiCl_3$ is pure) and a different stacking arrangement at the lateral surfaces of the crystals [24,37]. PP materials produced with both these catalysts have three highly isotactic components (Components *I* - *III* in Table **5**) and a small component with a low isotacticity degree (block-polymer). Two of the components, *II* and *III*, have practically the same stereoregularity parameters in both polymers whereas Component *I* in PP produced with δ-$TiCl_3$ has a noticeably higher isotacticity degree, [*mmmm*] ~0.978 vs. 0.969 for Component *I* in PP produced with γ-$TiCl_3$. This difference explains a nearly 2°C difference in the DSC peak positions of these components.

γ-$TiCl_3$ and VCl_3 have the same crystal structure but they differ in the lengths of the M–Cl and M–M bonds, 2.50 and 3.54 Å, respectively, for γ-$TiCl_3$ and 2.45 and 3.47 Å for VCl_3 [24,37]. A comparison of experimental DSC melting curves of these PP samples (Figures **9-A** and **9-C**) shows that the curves are very similar in shape. However, the whole curve of the VCl_3-derived PP is shifted to lower temperatures by ~2°C. DSC peak resolution (Figures **9-B** and **9-D**, Table **5**) shows that both polymers consist of four components. Components *I* - *III* represent the fractions of high isotacticity. They are present in both polymers in approximately the same proportions (Fr_i) but the stereoregularity parameters for each component are slightly lower in the polymer produced with VCl_3.

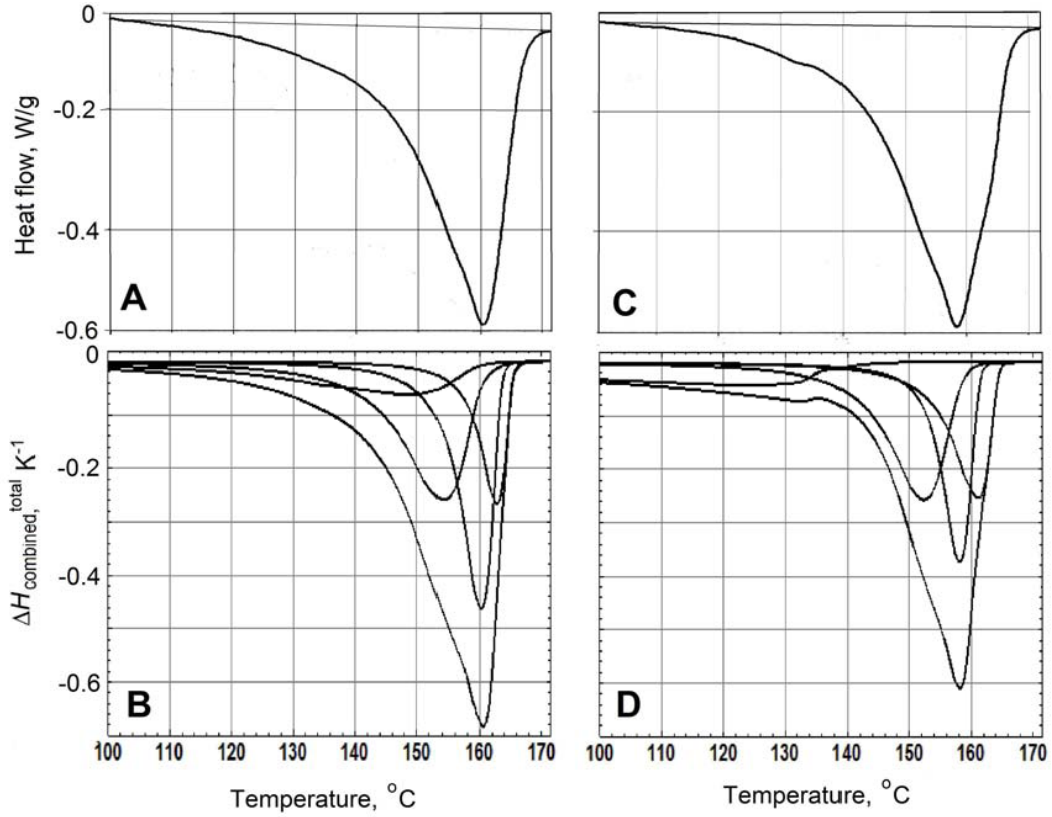

Figure 9: Modeling melting curves of isotactic PP. Experimental melting curves of PP prepared with Ziegler-Natta catalysts γ-$TiCl_3$ - $Al(C_2H_5)_3$ (**A**) and VCl_3 - $Al(C_2H_5)_3$ (**C**). **B** and **D** - modeling respective DSC curves with four components; Equations 13 and 15.

Apparently, these differences reflect small differences in the geometrical features of the active centers.

CONCLUSIONS

This paper describes a procedure for modeling DSC melting curves of PP produced with isospecific single-center and multi-center polymerization catalysts. The procedure is based on several principal assumptions:

1. Each peak on the DSC melting curve of a slowly crystallized/annealed PP sample represents melting of a particular polymer component characterized by a certain isotacticity level. The latter can be represented either by the conditional probability of isotactic linking, p_{iso}, or by the content of meso-pentads, [*mmmm*].

2. The distribution of isotactic blocks with respect to their length (the number of monomer units in the blocks) is calculated based on the enantiomorphic statistics of imperfectly isotactic chains.

3. Long propylene blocks crystallize in the folded morphology in the process of primary crystallization and form thick lamellae. The thickness of these lamellae is distributed according to the Gauss statistics.

4. Relatively short propylene blocks crystallize in a fully extended form and produce thin lamellae in the process of secondary crystallization.

Several modeling examples demonstrate that these assumptions are sufficient for an adequate representation of most characteristic features of DSC melting curves of isotactic PP. This approach, in principle, is similar to modeling the results of such modern analytical techniques as Tref [17-c] and Crystaf [18].

The DSC modeling process described here is semi-empirical; it requires the use of several adjustable parameters, most importantly, melting points of very thick lamellae (T_m^o in Equation 11) and the distribution width of thick lamellae, the σ parameter in Equation 11. The principal advantages of the modeling are the correct description of shapes of DSC melting curves, the physical interpretation of low-temperature tails in DSC curves of PP, and the ability to estimate relative

amounts of crystallizable material with a different stereoregularity degree in complex PP mixtures.

ACKNOWLEDGEMENTS

Sample of PP produced with supported Ziegler-Natta catalyst was presented by Dr. M. C. Sacchi (Istituto di Chimica delle Macromolecole del CNR, Milano, Italy). Dr. I. Mingozzi (Basell Polyolefine, Ferrara, Italy) carried out Tref analysis of this polymer and Dr. H. Fruitwala (ExxonMobil Chemical Company, Baytown, USA) performed its Crystaf analysis. Drs. P. M. Nedoresova and L. A. Rishina (Institute of Chemical Physics, Russian Academy of Science, Moscow, Russia) prepared samples of PP with the metallocene and post-metallocene catalysts.

APPENDIX

Position of the Maximum on a DSC Melting Curve

A Gauss distribution curve in the DSC coordinates is given by Equation 11:

$$\Delta H = T_m^{o}\cdot\chi/[(T_m^{o} - T)^2\cdot(\sigma\sqrt{2\pi})]\cdot\mathrm{Exp}\{-(T_m^{o}\cdot\chi)^2/2\sigma^2\cdot [(T_m^{o} - T_m^{av})^{-1} - (T_m^{o} - T)^{-1}]^2\} \text{ vs. } T \text{ (K)}$$

where T_m^{o} and T_m^{av} are in degree K. The maximum of this dependence is positioned at $d(\Delta H)/dT = 0$. The differentiation was performed with Mathematica 8 program:

$$T_{max}^{DSC}\,(°C) = [2.0\cdot(T_m^{o} - T_m^{limit})]^{-1}\,\{2.0\cdot(T_m^{o} - T_0)\cdot (T_m^{o} - T_m^{limit}) + 0.5\cdot[(T_m^{o} - T_0)\cdot(\chi/l_{step})/\sigma]^2 - \sqrt{0.5}\cdot \{(T_m^{o} - T_0)\cdot(\chi/l_{step})/\sigma]\cdot[4.0\cdot(T_m^{o} - T_m^{limit})^2 + 0.5\cdot[(T_m^{o} - T_0)\cdot(\chi/l_{step})/\sigma]^2\}^{0.5}\}$$

where T_m^{o} is in K, T_0 = 273.1°C, l_{step} = 2.17 Å and T_m^{limit} (K) is calculated as $T_m^{limit} \approx T_m^{o}\cdot[1 - (\chi/l_{step})/n_{limit})]$.

REFERENCES

[1] (a) Bensason S, Minick J, Moet A, Chum S, Hiltner A, Baer E. J Polym Sci Part B: Polym Phys 1996; 34: 1301. http://dx.doi.org/10.1002/(SICI)1099-0488(199605)34:7<1301::AID-POLB12>3.0.CO;2-E

(b) Bortolussi F, Broyer J-P, Spitz R, Boisson C. Macromol Chem Phys 2002; 203: 2501. http://dx.doi.org/10.1002/macp.200290032

(c) Piel C, Karssenberg FG, Kaminsky W, Mathot VBF. Macromolecules 2005; 38: 6789. http://dx.doi.org/10.1021/ma0505732

(d) Nomura K, Itagaki K, Fujiki M. Macromolecules 2005; 38: 2053. http://dx.doi.org/10.1021/ma050277p

(e) Aitola E, Puranen A, Setälä H, Lipponen S, Leskelä M, Repo T. J Polym Sci Part A: Polym Chem 2006; 44: 6569. http://dx.doi.org/10.1002/pola.21722

[2] Kissin YV. Alkene Polymerization Reactions with Transition Metal Catalysts. Amsterdam: Elsevier 2008, Chapter 2.

[3] Kissin YV. J Polym Sci, Part B: Polym Phys 2011; 49: 195. http://dx.doi.org/10.1002/polb.22164

[4] (a) De Rosa C, Auriemma F, DiCapua A, *et al*. J Am Chem Soc 2004; 126: 17040. http://dx.doi.org/10.1021/ja045684f

(b) De Rosa C, Auriemma F. Macromolecules 2006; 39: 249. http://dx.doi.org/10.1021/ma051228f

[5] (a) Nifantiev IE, Laishevtsev I, Ivchenko PV, *et al*. Macromol Chem Phys 2004; 205: 2275. http://dx.doi.org/10.1002/macp.200400238

(b) Resconi L, Guidotti S, Camurati I, *et al*. Macromol Chem Phys 2005; 206: 1405. http://dx.doi.org/10.1002/macp.200400533

[6] (a) Toyota A, Tsutsui T, Kashiwa N. J Molec Catal 1989; 56: 220. http://dx.doi.org/10.1016/0304-5102(89)80187-7

(b) Tsutsui T, Ishimaru N, Mizuno A, Toyota A, Kashiwa N. Polymer 1989; 30: 1350. http://dx.doi.org/10.1016/0032-3861(89)90059-1

(c) Chien JCW, Tsai WM, Rausch MD. J Am Chem Soc 1991; 113: 8570. http://dx.doi.org/10.1021/ja00022a081

[7] Kakugo M, Miyatake T, Naito Y, Mizunuma K. In: Quirk RP, editor. Transition Metal Catalyzed Polymerizations. Ziegler-Natta and Metathesis Polymerization. New York: Cambridge University Press 1988; p. 624.

[8] (a) Song W, Rausch MD, Chien JCW. J Polym Sci Part A: Polym Chem 1996; 34: 2945; (b) Marques MFV, Bastos QC. J Polym Sci Part A: Polym Chem 2005; 43: 263.

[9] (a) Naga N, Mizunuma K, Sadatoshi H, Kakugo M. Macromolecules 1997; 30: 2197. http://dx.doi.org/10.1021/ma961438f

(b) Ferreira ML, Galland GB, Damiani DE, Villar MA. J Polym Sci Part A: Polym Chem 2001; 39: 2005. http://dx.doi.org/10.1002/pola.1176

(c) Graef SM, Wahner UM, Van Reenen AJ, Brüll R, Sanderson RD, Pasch H. J Polym Sci Part A: Polym Chem 2002; 40: 128. http://dx.doi.org/10.1002/pola.10093

(d) Palza H, Lopez-Majada M, Quijada R, Benavente R, Perez E, Cerrada ML. Macromol Chem Phys 2005; 206: 1221. http://dx.doi.org/10.1002/macp.200500036

(e) Rulhoff S, Kaminsky W. Macromol Chem Phys 2006; 207: 1450. http://dx.doi.org/10.1002/macp.200600176

[10] (a) Venditto V, De Tullio G, Izzo L, Oliva L. Macromolecules 1998; 31: 4027. http://dx.doi.org/10.1021/ma971908l

(b) Abbondanza L, Abis L, Cardi N, Garbassi F, Po R. Macromol Chem Phys 2003; 204: 1428. http://dx.doi.org/10.1002/macp.200350009

[11] Samuels RJ. J Polym Sci Polym Phys 1975; 13: 1417. http://dx.doi.org/10.1002/pol.1975.180130713

[12] (a) Corradini P, Napolitano R, Oliva L, Petraccone V, Pirozzi B, Guerra G. Makromol Chem Rapid Comm 1982; 3: 753. http://dx.doi.org/10.1002/marc.1982.030031018

(b) Guerra G, Petraccone V, Corradini P, *et al*. J Polym Sci: Polym Phys Ed 1984; 22: 1029. http://dx.doi.org/10.1002/pol.1984.180220608

[13] (a) Petraccone V, Guerra G, De Rosa C, Tuzi A. Makromol Chem Rapid Comm 1984; 5: 631. http://dx.doi.org/10.1002/marc.1984.030051003

(b) Petraccone V, Guerra G, De Rosa C, Tuzi A. Macromolecules 1985; 18: 813. http://dx.doi.org/10.1021/ma00146a037

[14] Paukkeri R, Lehtinen A. Polymer 1993; 34: 4075-4083. http://dx.doi.org/10.1016/0032-3861(93)90669-2

[15] Celli A, Fichera A, Marega C, Marigo C, Paganetto G, Zannetti R. Eur Polym J 1993; 29: 1037. http://dx.doi.org/10.1016/0014-3057(93)90305-Y

[16] Yadav YS, Jain PC. Polymer 1986; 27: 721. http://dx.doi.org/10.1016/0032-3861(86)90130-8

[17] (a) Passingham C, Hendra PJ, Cudby MA, Zichy V, Weller M. Eur Polym J 1990; 26: 631. http://dx.doi.org/10.1016/0014-3057(90)90219-T

(b) Zhu X, Yan D, Tan S, Wang T, Yan D, Zhou E. J Appl Polym Sci 2000; 77: 163. http://dx.doi.org/10.1002/(SICI)1097-4628(20000705)77:1<163::AID-APP22>3.0.CO;2-L

(c) Zhang Z, Gong Y, He T. Eur Polym J 2003; 39: 2315. http://dx.doi.org/10.1016/j.eurpolymj.2003.08.001

[18] Pasquini N. Polypropylene Handbook, 2nd ed. Cincinnati: Hanser Gardner Publ 2005.

[19] Bond EB, Spruiell JE, Lin JS. J Polym Sci Part B: Polym Phys 1999; 37: 3050. http://dx.doi.org/10.1002/(SICI)1099-0488(19991101)37:21<3050::AID-POLB14>3.0.CO;2-L

[20] (a) Campbell RA, Phillips PJ. Polymer 1993; 34: 4809. http://dx.doi.org/10.1016/0032-3861(93)90002-R

(b) Yan RJ, Jiang B. J Polym Sci Polym Phys 1993; 31: 1089. http://dx.doi.org/10.1002/polb.1993.090310904

(c) Thomann R, Wang C, Kressler J, Mülhaupt R. Macromolecules 1996; 29: 8425. http://dx.doi.org/10.1021/ma951885f

[21] (a) Li JX, Cheung WL, Jia DM. Polymer 1999; 40: 1219. http://dx.doi.org/10.1016/S0032-3861(98)00345-0

(b) Hosier IL, Alamo RG, Lin JS. Polymer 2004; 45: 3441. http://dx.doi.org/10.1016/j.polymer.2004.02.071

(c) Nedkov E, Dobreva T. Eur Polym J 2004; 40: 2573. http://dx.doi.org/10.1016/j.eurpolymj.2004.06.017

(d) Juhász P, Varga J, Belina K, Marand H. J Therm Anal Calorim 2004; 69: 561. http://dx.doi.org/10.1023/A:1019916007954

(e) Qiang Z, Yonggang S, Shouke Y, Yihu S, Mao P, Zhang Q. Polymer 2005; 46: 3163. http://dx.doi.org/10.1016/j.polymer.2005.01.097

[22] De Rosa C, Auriemma F. Polym Chem 2011; 2: 2155. http://dx.doi.org/10.1039/c1py00129a

[23] Rishina LA, Galashina NM, Nedorezova PM, *et al*. Vysokomol Soed 2004; A46: 1493.

[24] Kissin YV. Alkene Polymerization Reactions with Transition Metal Catalysts. Amsterdam: Elsevier 2008, Chapter 4.

[25] Rishina LA, Galashina NM, Gagieva SC, Tuskaev VA, Kissin YV. Eur Polym J 2013; 49: 145.

[26] Press K, Cohen A, Goldberg I, Venditto V, Mazzeo M, Kol M. Angew Chem Int Ed 2011; 50: 3529. http://dx.doi.org/10.1002/anie.201007678

[27] (a) Shelden RA, Fueno T, Tsunetsugu T, Furukawa J. J Polym Sci Part A 1965; 3: 27; (b) Shelden RA, Fueno T, Furukawa J. J Polym Sci Polym Phys Ed 1969; 7: 763.

[28] Kissin YV. Alkene Polymerization Reactions with Transition Metal Catalysts. Amsterdam: Elsevier 2008, Chapter 3.

[29] Soares JBP, Hamielec AE. Polymer 1995; 36: 1639. http://dx.doi.org/10.1016/0032-3861(95)99010-R

[30] Spieckermann F, Wilhelm H, Kerber M, *et al*. Polymer 2010; 51: 4195. http://dx.doi.org/10.1016/j.polymer.2010.07.009

[31] (a) Barham PJ, Chivers RA, Jarvis DA, Martinez-Salazar J, Keller A. J Polym Sci Polym Lett Ed 1981; 19: 539. http://dx.doi.org/10.1002/pol.1981.130191104

(b) Barham PJ, Jarvis DA, Keller A. J Polym Sci Polym Phys Ed 1982; 20: 1733. http://dx.doi.org/10.1002/pol.1982.180200922

(c) Chivers RA, Barham PJ, Martinez-Salazar D, Keller A. J Polym Sci Polym Phys Ed 1982; 20: 1717. http://dx.doi.org/10.1002/pol.1982.180200921

(d) Wunderlich B. Macromolecular Physics. New York: Academic Press 1980; vol. 3.

[32] (a) Mezghani KK, Campbell RA, Phillips PJ. Macromolecules 1994; 27: 997. http://dx.doi.org/10.1021/ma00082a017

(b) Yamada K, Hikosaka M, Toda A, Yamazaki S, Tagashira K. Macromolecules 2003; 36: 4790. http://dx.doi.org/10.1021/ma021206i

[33] Monakhova TV, Nedorezova PM, Tsvetkova VM, Shlyapnikov YA. Vysokomol Soed 2005; A46: 1.

[34] Arranz-Andrés J, Peña B, Benavente R, Pérez E, Cerrada ML. Eur Polym J 2007; 43: 2357. http://dx.doi.org/10.1016/j.eurpolymj.2007.03.034

[35] Kissin YV, Chadwick JC, Mingozzi I, Morini G. Macromol Chem Phys 2006; 207: 1344. http://dx.doi.org/10.1002/macp.200600074

[36] Kissin YV, Fruitwala HA. J Appl Polym Sci 2007; 106: 3872. http://dx.doi.org/10.1002/app.27090

[37] (a) Natta G, Corradini P, Allegra G. J Polym Sci 1961; 51: 399. http://dx.doi.org/10.1002/pol.1961.1205115602

(b) Giudetti G, Zannetti R, Ajo D, Marigo A, Vidali M. Eur Polym J 1980; 16: 1007. http://dx.doi.org/10.1016/0014-3057(80)90184-6

Received on 24-02-2013 Accepted on 15-03-2013 Published on 31-03-2013

DOI: http://dx.doi.org/10.6000/1929-5995.2013.02.01.2